13. T. R. Quinn, S. D. Tremaine, M. Duncan, *Astron. J.* **101**, 2287 (1991).
14. G. Balmino, B. Moynot, N. Vales, *J. Geophys. Res.* **87**, 9735 (1982).
15. W. M. Kaula, N. H. Sleep, R. J. Phillips, *Geophys. Res. Lett.* **16**, 1333 (1989).
16. W. M. Kaula, *ibid.* **6**, 194 (1979).
17. M. Standish, personal communication.
18. M. E. Davies *et al.*, *Celest. Mech.* **22**, 205 (1980).
19. M. E. Davies *et al.*, *ibid.* **46**, 187 (1989).
20. J. Touma and J. Wisdom, in preparation.
21. J. Wisdom and M. Holman, *Astron. J.* **102**, 1528 (1991).
22. _____, *ibid.* **104**, 2022 (1992).
23. W. R. Ward, in *Mars*, H. H. Kiefer, B. M. Jacosky, C. W. Snyder, M. S. Matthews, Eds. (Univ. of Arizona Press, Tucson, 1992).
24. B. V. Chirikov, *Phys. Rep.* **52**, 263 (1979).
25. J. Wisdom, *Icarus* **63**, 272 (1985).
26. D. Escande, in *Plasma Theory and Nonlinear and Turbulent Processes in Physics*, V. G. Baryakhtar, V. M Chernousenko, N. S. Erokhin, A. G. Sitenko, V. E. Zakharov, Eds. (World Scientific, Singapore, 1988).
27. D. P. Rubicam, *Science* **248**, 720 (1990).
28. This research was supported in part by NSF Presidential Young Investigator Award AST-887365, in part by the NASA Planetary Geology and Geophysics Program under grant NAGW-706, and in part by the National Science Foundation under grant MIP-9001651. We thank M. Standish for assistance with initial conditions. We thank M. Holman, S. D. Tremaine, and S. J. Peale for valuable discussions.

16 December 1992; accepted 15 January 1993

# Lidar Observations of the Meteoric Deposition of Mesospheric Metals

Timothy J. Kane and Chester S. Gardner*

The mesospheric sodium and iron layers at an altitude between about 80 and 110 kilometers are routinely monitored by atmospheric physicists using resonance fluorescence lidar techniques because these constituents are excellent tracers of mesopause chemistry and dynamics. The mesospheric metals are the products of meteoric ablation. Existing ablation profiles are model calculations based in part on radar observations of the ionized background atmosphere left in the wake of high-speed (>20 kilometers per second) meteoroids. Thin trails of neutral metal atoms, ablated from individual meteoroids, are occasionally observed with high-power lidars. The vertical distribution of 101 sodium and 5 iron meteor trails observed during the past 4 years at Urbana, Illinois; Arecibo, Puerto Rico; and near Hawaii is approximately Gaussian in shape with a centroid height of 89.0 (±0.3) kilometers and a root-mean-square width of 3.3 (±0.2) kilometers. This directly measured ablation profile is nearly the same as the mean iron layer profile but is considerably different from existing models and the distribution of ionized meteor trails observed by radars. A lower limit on the influx to the mesopause region from the lidar meteors is approximately $1.6 \times 10^3$ sodium and $2.7 \times 10^4$ iron atoms per second per square centimeter, which corresponds to an annual flux of meteoric debris into the mesosphere of about 2.0 (±0.6) gigagrams. Because the lidars can detect only the ablation trails left by the larger meteors, the observations suggest that the actual meteoric influx may be larger than the more recently reported values, which range between 16 and 78 gigagrams per year.

For more than 20 years resonance fluorescence lidar techniques have been used to study the chemistry and dynamics of the atomic metal layers in the height range between 80 and 110 km. Meteoric ablation is the major source of these layers, and photo-ionization in the lower thermosphere and chemical reactions involving O, $O_2$, $O_3$, and $CO_2$ below the mesopause are the major sinks. The seasonal variations in Na and Fe abundances, which are both minima in summer, are believed to be related to the temperature dependencies of the sink reactions, which are more efficient at the lower summertime temperatures of the mesopause. The predicted increases of atmospheric $CO_2$ during the next century and the accompanying increases in radiative cooling (*1*) are likely to have major effects on the concentrations and vertical distributions of the mesospheric metal layers. In fact, Clemesha *et al.* (*2*) recently reported a long-term decrease in the height of the Na layer at Sao Jose dos Campos, Brazil, which averaged 49 (±12) m year$^{-1}$ from 1972 to 1987. These researchers suggested that this change is consistent with long-term cooling trends detected by other techniques and predicted by models that incorporate the expected increases in middle atmosphere $CO_2$ and $CH_4$ concentrations.

The metal layers are also of interest because they serve as tracers of the thermal and dynamic state of the upper atmosphere. Narrow band Na lidars are now being used to measure mesopause temperature and Doppler wind profiles (*3*) and the technology exists to make similar observations by probing other metal species. The Na layer is also of considerable current interest to optical astronomers who are now developing laser guide star technology for adaptive image compensation in ground-based telescopes (*4*, *5*). In this technology, powerful lasers are used to create bright artificial stars in the Na layer, which provide the reference wave front for the adaptive imaging systems.

Knowledge of the meteoric source distribution of the mesospheric metals is essential for understanding their chemical evolution. The high vertical and temporal resolution achieved with modern high-power lidars facilitates the observation of what are apparently trails left by ablating meteors. These trails are very thin [~100 m full width at half maximum (FWHM)] and short-lived, remaining in the lidar system's 1-mrad field of view (FOV) for typically less than 30 s. The peak atomic densities in these trails can be quite large, reaching $10^4$ cm$^{-3}$ for Na and $10^5$ cm$^{-3}$ for Fe. The most likely source of these events is the recent ablation of a metal-rich meteoroid. To date, various lidars operated by our group have observed 101 Na and 5 Fe meteor trails. The altitude distribution of these events is considerably different from that of theoretical models of the meteoric ablation profile and the distribution of ionized meteor trails observed by radars. Trails observed by the lidars contribute at least 10% of the commonly accepted value for the total Na and Fe influx to the mesosphere.

Most of the data reported here were obtained at the Urbana Atmospheric Observatory (40°N, 88°W), with a tunable dye laser that was capable of making nighttime measurements of the altitude distributions of mesospheric Na, Fe, Ca, and $Ca^+$ (*6*, *7*). This system typically operates with a vertical resolution of 37.5 or 48 m (depending on computer configuration) and a temporal resolution of 30 s for Na observations and 3 min for Fe, Ca, and $Ca^+$ observations. This lidar was used to study the mesospheric Na layer at Urbana in 1988 and 1989 and at Arecibo, Puerto Rico, in the spring of 1989. This system was also used to make airborne Na lidar observations in Hawaii in March and April 1990. During the past year the system has been used for Fe, Ca, and $Ca^+$ observations at Urbana. The Na Doppler-temperature lidar is a narrow band system that can be used to measure line-of-sight winds and temperatures at mesopause heights by probing the fine structure of the Na $D_2$ resonance line (*3*). Only the Na density profiles obtained by this system, with its resolution of 48 m and 1 min, are reported here. All of the University of Illinois lidars have a full-width beam divergence of about 1 mrad. The lidars are thus probing a patch of the atmosphere about 100 m in diameter at an

Department of Electrical and Computer Engineering, University of Illinois at Urbana–Champaign, Urbana, IL 61801.

*To whom correspondence should be addressed

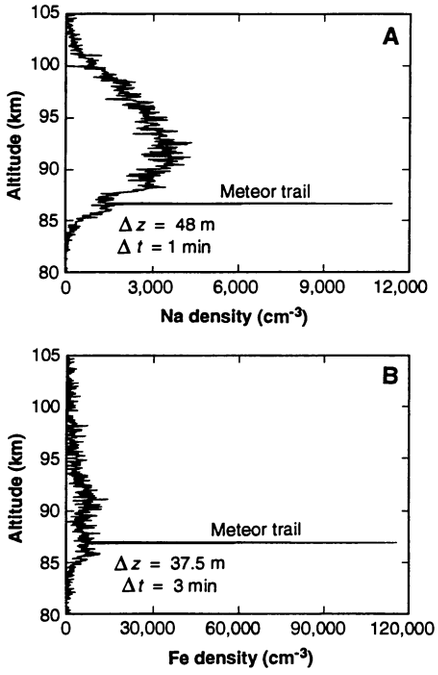


**Fig. 1.** Density profiles of (**A**) Na and (**B**) Fe measured simultaneously on 25 November 1991 (2254 LT) at Urbana; $\Delta z$ = vertical resolution. The thin dense layers near 86.5-km altitude are believed to be meteor ablation trails.

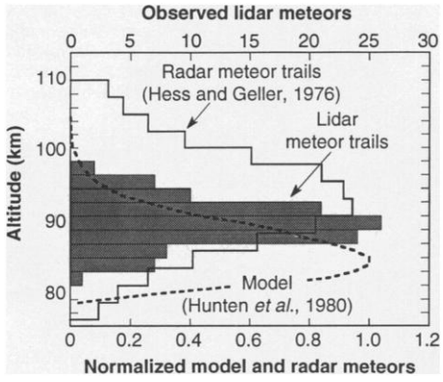


**Fig. 2.** Altitude histogram of 106 lidar meteor trails in 2-km range bins plotted along with a theoretical model of the meteoric deposition profile and the distribution of radar meteors at Urbana.

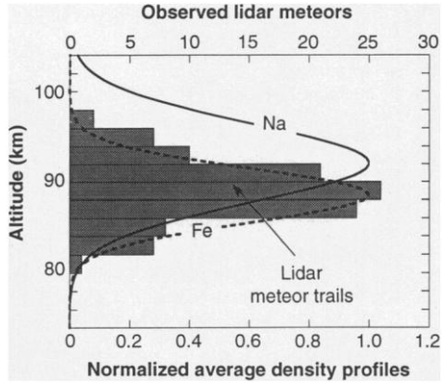


**Fig. 3.** Altitude histogram of 106 lidar meteor trails plotted along with the average normalized density profiles of mesospheric Na and Fe at Urbana.

altitude of 100 km. During a total observing time of 1084 hours with these various systems, 106 meteor trails were observed.

Density profiles of Na and Fe obtained simultaneously on the evening of 25 November 1991 at Urbana exhibit meteor trails at nearly identical altitudes (Fig. 1). Both trails were within the FOV of the receiving telescope for less than 2 min and were ~100 m thick FWHM. We believe these Na and Fe trails originated from the same meteoroid. However, Fe meteor trails have been observed on several occasions at Urbana when Na meteor trails were not. This is not surprising because the Na content in certain iron meteorites has been found to be extremely low (*8*).

If the Na and Fe trails shown in Fig. 1 originated from the same meteoroid, the ratio of the Na and Fe abundances in the trails should yield the relative abundances of these metals in the meteoroid of origin, provided that the data are corrected for the different integration times. For the Na Doppler-temperature lidar, each Na profile requires a 60-s acquisition time and then the laser is tuned to a different frequency within the $D_2$ fluorescence spectrum. The total tuning time before and after the profile in Fig. 1 was collected was 40 s, so that the total duration $\tau$ of the Na meteor trail was less than or equal to 100 s. The observed density of the Na meteor trail equals the true density only if $\tau > 60$ s. The observed density equals $\tau/60$ s times the true density if $\tau < 60$ s. The Fe integration time was 180 s, and the Fe meteor trail duration was less than this value. The ratio of the observed abundance of Fe to Na was 10.6. By taking into account the different integration times, we calculate that the ratio of the actual Fe abundance to the actual Na abundance in the meteoroid was between 19 and 32. The average atomic ratio of Fe to Na in chondritic meteorites is about 17 (*8*, *9*).

The bulk of the meteor trail data presented here is from our ground-based Na lidar studies. The high aircraft velocity for the Hawaii airborne data and the long integration time of the Fe lidar inhibit the detection of meteor trails with these systems. Figure 2 is a histogram showing the height distribution of the meteor trails. We calculated the centroid height [89.0 (±0.3) km] and the root-mean-square (rms) width of the distribution [3.3 (±0.2) km] using the individual event data (not the histogram).

A model meteor ablation profile (*10*) and a distribution of radar meteor echoes from Urbana (*11*) are also plotted in Fig. 2. The model is for the deposition of meteoric debris, including dust and molecules as well as individual atoms and ions. The altitude distribution of this model is a function of meteoroid velocity with faster moving meteoroids ablating at higher altitudes. Meteor radars "observe" the ionized background atmosphere in the wake of a meteoroid. The ionization efficiency of a meteoroid increases considerably above velocities of 20 km $s^{-1}$ (*12*). The bottom edge of the radar meteor distribution shown in Fig. 2 cuts off where the meteoroid velocities drop below the ionization threshold of 20 km $s^{-1}$.

Most of the metallic atoms ablated from a meteoroid are neutral (*13*). Diffusion and chemical reactions will disperse and deplete the atomic meteor trails within a few minutes after ablation. The molecular diffusivity at mesopause heights is on the order of 5 $m^2$ $s^{-1}$, whereas eddy diffusivity is approximately 100 $m^2$ $s^{-1}$. The scale height of the observed meteor trails is on the order of 50 m. Thus, the effective diffusion velocities are on the order of a few tens of centimeters per second to a few meters per second and could spread the meteor trails by 1 km in as little as 10 min, making them difficult to detect. We believe that the thin trails we have observed ablated only seconds or at most a few minutes before they were detected by the lidar. In addition to undergoing diffusion, the metallic atoms are quickly incorporated into molecules through various chemical reactions. For Na, the pertinent sink reaction is

$$Na + O_2 + M \rightarrow NaO_2 + M \quad (1)$$

which is considerably faster at lower altitudes, where the atmospheric density is greater, than at higher altitudes. The time constant of this reaction is a few minutes at 90 km but only a few seconds at 80 km (*14*). Consequently, meteor atoms deposited near 90 km have a far greater chance of being observed by the lidar than those deposited below 80 km. This behavior is apparent in the lidar meteor trail distribution of Fig. 3. The Na atoms ablated below 80 km react quickly to form compounds that cannot be detected by the lidar. Meteoric deposition and ionization still occur below 80 km, as seen in the ablation model and the radar meteor distribution. The top side of the lidar meteor trail distribution, which is similar in shape to the model, may actually be the ablation profile as determined by the velocity distribution of incoming meteoroids. The radar meteors are observable well above either the lidar meteors or the ablation model. It is believed that, although the meteoroids can ionize the atmosphere at such high altitudes, it is only in the denser, lower atmosphere that there is

**Table 1.** Comparison of average Fe and Na layer profiles to the meteor trail distribution.

| Value | Centroid height (km) | Width (rms) (km) | Abundance ($10^9$ cm$^{-2}$) |
|---|---|---|---|
| Meteor trail distribution | 89.0 (±0.3) | 3.3 (±0.2) | |
| Average Fe layer profile | 88.1 | 3.4 | 10.6 |
| Average Na layer profile | 92.1 | 4.4 | 5.4 |

**Table 2.** Characteristics of several long-duration lidar meteor trails; LT, local time.

| Date | Location | Initial time (LT) | Abundance ($10^7$ cm$^{-2}$) | Peak density (cm$^{-3}$) | Duration (min) | Vertical velocity (m s$^{-1}$) |
|---|---|---|---|---|---|---|
| 3/4/88 | Urbana | 2117 | 2.5 | 2400 | 3.5 to 4.5 | −4.4 |
| 3/4/88 | Urbana | 2257 | 3.2 | 3000 | 1 to 2 | +5.1 |
| 4/16/88 | Urbana | 0116 | 3.3 | 2500 | 2.5 to 3.5 | 0 |
| 7/28/88 | Urbana | 2320 | 1.8 | 1500 | 1 to 2 | −3.4 |
| 3/26/89 | Arecibo | 2044 | 3.0 | 2500 | 2 to 3 | −4.7 |

sufficient friction to actually result in ablation (*13*).

Figure 3 shows the same lidar meteor trail height distribution as Fig. 2 but plotted with the average Na and Fe density profiles at Urbana (*15*). Table 1 lists the layer parameters for these profiles. The background Fe layer shape is remarkably similar to the incoming meteoric flux, but the average Na layer is a few kilometers higher in altitude. Although the observed lidar meteor distribution is composed primarily of Na trails and altitude-dependent chemistry will affect the detectability of trails composed of different species, it is reasonable to assume that the Fe and Na ablation profiles are similar in shape. Vertical transport caused by eddy diffusion will redistribute the ablated atoms during their mean lifetime in the mesosphere. The mean lifetime of a metal atom in the mesosphere is defined as the average time between meteoric deposition and subsequent precipitation to lower altitudes as part of heavier molecules. If the mean lifetime of the metal species is long with respect to the time scales associated with the vertical transport, the observed distribution of the species could be quite different from the source distribution in Fig. 3. The separation in altitude between the average Na layer and the source distribution from Table 1 is about 3.1 km. To achieve this type of drift from the source would require a mean Na lifetime of ~30 hours, if we assume the source distribution scale height is ~3.3 km and the typical eddy diffusivity at mesopause heights is ~100 m$^2$ s$^{-1}$.

The Na lifetime has been estimated by another approach to be about 50 hours (*15*). Although diffusion transports the Na downward as well as upward, the sink reaction (Eq. 1) quickly depletes atomic Na at the lower altitudes. If the mean lifetime of the metal species is short with respect to vertical transport effects, the species will be distributed much like the source. This appears to be the case for mesospheric Fe. The mean lifetime of this constituent is approximately 6 hours (*15*). Diffusive transport during the lifetime of an Fe atom is estimated to be about 0.7 km. The mean Fe layer is actually 0.9 km lower than the observed meteor trail distribution.

Because the meteor trails are generally within the FOV of the lidar for less than the profile integration period, little can be said about their abundances and vertical motion. There are occasions, however, when a meteor trail is observed in adjacent lidar profiles. Because these trails are within the lidar's FOV for at least one integration period, we know that the observed density is equal to the true density. Listed in Table 2 are the characteristics of four such events observed at Urbana and one observed at Arecibo. The average abundance and peak density of these long-lived meteor trails are $2.8 \times 10^7$ (±0.6) cm$^{-2}$ and 2400 (±500) cm$^{-3}$, respectively. The average magnitude of the apparent vertical velocities of these trails is 3.5 m s$^{-1}$.

An estimate of the meteoric input of metals to the mesosphere can be calculated from the above results. Because longer integration times decrease the sensitivity of the lidar to meteor detection, we shall restrict our attention to the Na lidar data acquired at 30-s integration periods. A total of 89 events were observed in 450 hours of total operating time, yielding an average observation rate of 0.20 (±0.05) meteor per hour. Multiplying the average trail abundance by the average event rate yields an input flux of atomic Na from lidar meteors (observed with 30-s integration periods) of approximately 1600 (±500) atom s$^{-1}$ cm$^{-2}$. This is smaller by about a factor of 10 than the typical Na influx quoted in the literature [$\sim 1.3 \times 10^4$ atom s$^{-1}$ cm$^{-2}$ (*14*)]. Assuming that Na makes up about 0.5% of meteoric debris by mass (*8*), we calculate that the annual flux of meteoric debris into the mesosphere is about 2.0 (±0.6) Gg, which is smaller than the values of 16 Gg calculated by Hughes (*16*) and 78 Gg calculated by Wasson and Kyte (*17*). Because the ratio of Fe to Na in meteoroids is ~17, the lower limit for the total Fe flux due to meteors is $2.7 (\pm 0.9) \times 10^5$ atom s$^{-1}$ cm$^{-2}$.

Because the telescope FOV is extremely small (100-m diameter at 100-km altitude), only a small fraction of the total meteor flux is observed by the lidar. The detection threshold for Na trails is about 500 atom cm$^{-3}$. Horizontal advection of a meteor trail by the background wind field can substantially reduce its detectability. Horizontal winds at mesopause heights average about 30 m s$^{-1}$. If the wind is oriented normal to the trajectory of the meteor trail, the trail will remain in the lidar FOV for only a few seconds so that the apparent density will be significantly less than the true density. If the wind is oriented along the trail, meteors with entry trajectories near nadir will appear to have high vertical velocities and will be advected through many range bins during the integration period. Four of the five trails listed in Table 2 exhibit moderate apparent vertical velocities. On the basis of the characteristics of these long duration trails, we believe that the lidars are observing primarily those meteors whose trajectories are within about 30° of the horizontal and oriented approximately in the direction of the mean wind. The initial mass of many of the meteors contributing to the influx may be too small to permit the ablation trails to be detected by the lidar, regardless of their trajectories and the data integration time. Therefore, we believe the lidar observations provide an extreme lower bound on the calculated influx.

These data on lidar meteor trails provide new insights into the origin of the atomic metal layers in the mesosphere. A thorough understanding of the chemistry and dynamics of these layers can be realized only if the meteoric source distribution is known. The lidar measurements challenge current estimates of both the amount and altitude distribution of the influx of the meteoric metals.

## REFERENCES AND NOTES


1. R. G. Roble and R. E. Dickinson, *Geophys. Res. Lett.* **16**, 1441 (1989).
2. B. R. Clemesha, V. W. J. H. Kirchhoff, D. M. Simonich, H. Takahashi, *ibid.* **5**, 873 (1978).
3. R. E. Bills, C. S. Gardner, S. J. Franke, *J. Geophys. Res.* **96**, 22701 (1991).
4. C. S. Gardner, B. M. Welsh, L. A. Thompson, *Proc. IEEE* **78**, 1721 (1990).
5. R. Q. Fugate *et al.*, *Nature* **353**, 144 (1991).
6. T. J. Beatty, R. E. Bills, K. H. Kwon, C. S. Gardner, *Geophys. Res. Lett.* **15**, 1137 (1988).
7. T. J. Kane, P. H. Mui, C. S. Gardner, *ibid.* **19**, 405 (1992).
8. B. Mason, Ed., *Handbook of Elemental Abundances in Meteorites* (Gordon & Breach, New York, 1971).

9. D. W. R. McKinley, *Meteor Science and Engineering* (McGraw-Hill, New York, 1961).
10. D. M. Hunten, R. P. Turco, O. B. Toon, *J. Atmos. Sci.* **37**, 1342 (1980).
11. G. C. Hess and M. A. Geller, *Aeron. Rep. 74* (Aeronomy Laboratory, Department of Electrical and Computer Engineering, University of Illinois, Urbana, 1976).
12. D. W. Hughes, *Space Res.* **15**, 531 (1975).
13. V. A. Bronshten, *Physics of Meteoric Phenomena* (Reidel, Dordrecht, Holland, 1983).
14. J. M. C. Plane, *Int. Rev. Phys. Chem.* **10**, 55 (1991).
15. T. J. Kane and C. S. Gardner, in preparation.
16. D. W. Hughes, in *Cosmic Dust*, J. A. M. McDonnell, Ed. (Wiley, New York, 1978), pp. 148–157.
17. J. T. Wasson and F. T. Kyte, *Geophys. Res. Lett.* **14**, 779 (1987).
18. We thank T. J. Beatty, R. E. Bills, R. L. Collins, C. A. Hostetler, W. M. Pfenninger, J. Qian, D. C. Senft, and D. R. Scherrer for help in system development and data acquisition. This work was supported in part by NSF grants ATM 88-11771, ATM 90-24367, and ATM 90-01511.

1 September 1992; accepted 23 December 1992

# Isomers of Small Carbon Cluster Anions: Linear Chains with up to 20 Atoms

Gert von Helden, Paul R. Kemper, Nigel G. Gotts, Michael T. Bowers*

**The structure of small carbon cluster anions, $C_n^-$ ($4 \leq n \leq 20$), was investigated with the use of ion chromatography. With this technique, both the existence and the relative amounts of possible structural isomers can be determined. More than 99% of the ions $C_5^-$ to $C_9^-$ were found to be linear under these experimental conditions. Starting with $C_{10}^-$, a monocyclic isomer was observed, and linear and moncyclic structures coexisted from $C_{10}^-$ through at least $C_{20}^-$. This result is in contrast to previous work on positive ions, which showed the existence of linear isomers from $C_5^+$ to $C_{10}^+$, with linear and cyclic isomers coexisting only from $C_7^+$ to $C_{10}^+$. Above $C_{10}^+$, no linear clusters were observed.**

During the last several years, considerable research effort has been directed toward understanding the structures and properties of small clusters. Small carbon clusters are especially interesting because of their possible importance in combustion and pyrolysis processes (*1*), their importance in astrophysical processes (*2*), and their role in the formation and growth of fullerenes. Because of their high reactivity, most carbon clusters cannot be isolated in macroscopic quantities and analyzed by traditional means. As a consequence, little is known about the structure of most clusters. Some structural information has been deduced from size distributions in mass spectra (*3*) and metastable reactions in mass spectrometers (*4*), reactivity studies (*5*), computational studies (*6–8*), and various spectroscopic techniques (*9*). Photoelectron spectroscopy (*10, 11*) shows the presence of linear clusters for cluster anions with as many as nine atoms and suggests that larger clusters have monocyclic ring structures with the possibility of both linear and cyclic structures being present in $C_{10}^-$ and $C_{11}^-$. Even with these results, it has remained unclear if cyclic cluster anions exist with less than 10 atoms or if linear clusters exist with more than 11 atoms and if there is a region where linear and cyclic clusters coexist. Coulomb explosion experiments (*12*) have shown the possible presence of different isomers for $C_4^-$, $C_5^-$, and $C_6^-$. A review on the research up to 1989 has been given by Weltner and van Zee (*9*).

We recently introduced the technique of ion chromatography and applied it to carbon cluster cations (*13*). This technique, in combination with computer modeling, allows us to probe the shape and possible existence of structural isomers for small cluster ions. Various families of structural isomers have been identified for carbon cluster cations (*13–15*). Here, we present results from similar studies on carbon cluster anions that contained from 4 to 20 atoms.

The experimental setup has been described previously (*16*), and only a brief outline is given here. A schematic of the apparatus is shown in Fig. 1. Carbon cluster anions are generated in a standard laser vaporization–supersonic expansion cluster source. A pulse of photons from an excimer laser impinges on a continuously rotating and translating graphite rod. The pulse is timed to coincide with a burst of helium, which is admitted from a pulsed valve. Carbon clusters exit the source through a 30-degree conical nozzle after traveling through a channel that is 3 mm in length and 2 mm in diameter. In some experiments, a spacer is inserted to increase the channel length to 8 mm. No further ionization is used. Cluster anions are accelerated to 5 keV and then mass-selected by a reverse geometry, double-focusing mass spectrometer. An electric shutter cuts a short pulse (2 to 10 μs) of ions out of the ≈40-μs mass-selected ion packet and injects it at low energies (2 to 15 eV) into a high-pressure drift cell (Fig. 2) filled with helium at 2 to 5 torr. A small electric field (2 to 20 V/cm) pulls the ions gently through the cell. Ions exiting the cell are passed through a quadrupole mass filter and are detected as a function of time. The resulting arrival time distribution (ATD) is collected on a multichannel scaler. The time an ion spends in the cell is inversely proportional to the mobility of the ion and directly proportional to the average cross section of the ion. Ions of the same mass but with different structures may have different mobilities. Structures with a large average cross section have a lower mobility

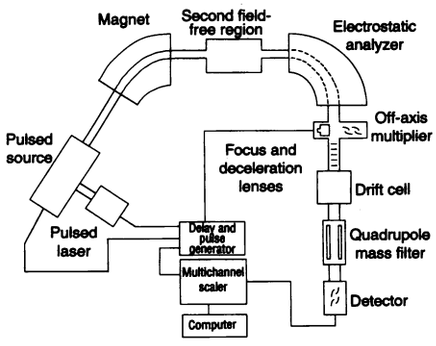


**Fig. 1.** Schematic of the overall ion chromatography instrument. Carbon cluster ions are generated by laser vaporization–supersonic expansion. Ions are mass-selected by the magnet and electrostatic analyzer and injected at low energy into the chromatography cell. Ions exiting the cell pass a quadrupole mass filter and are detected by standard ion counting techniques.

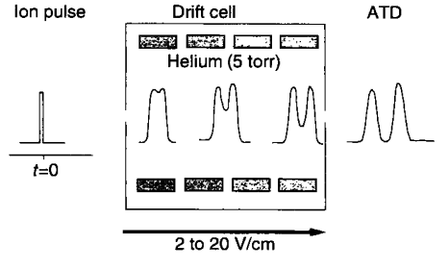


**Fig. 2.** Schematic of a typical ion chromatography experiment. A 5-μs ion packet is injected at low energy into the high-pressure drift cell. Ions drift through the cell under the influence of a weak electric field. Different structural isomers are separated because of their different collision cross section (size). Ions exiting the cell are recorded, and their ATDs are obtained. Typical drift times ($t$) in our cell were 100 to 1000 μs.

Department of Chemistry, University of California, Santa Barbara, CA 93106.

*To whom correspondence should be addressed.